Chinese Journal of
POLYMER SCIENCE 高分子科学

Mechanical Properties of Interlocked-ring Polymers: A Molecular Dynamics Simulation Study

Wu Zheng-Tao, Zhou Jia-Jia

Cite this article as:
Wu Zheng-Tao, Zhou Jia-Jia. Mechanical Properties of Interlocked-ring Polymers: A Molecular Dynamics Simulation Study[J]. *Chinese J. Polym. Sci*, 2019, 37(12): 1298-1304. doi: 10.1007/s10118-019-2279-z

View online: https://doi.org/10.1007/s10118-019-2279-z

Chinese Journal of
POLYMER SCIENCE

ARTICLE

https://doi.org/10.1007/s10118-019-2279-z
Chinese J. Polym. Sci. **2019**, *37*, 1298–1304

Mechanical Properties of Interlocked-ring Polymers: A Molecular Dynamics Simulation Study

Zheng-Tao Wu[a] and Jia-Jia Zhou[b*]

[a] *College of Engineering, Zhejiang Normal University, Jinhua 321004, China*
[b] *School of Chemistry, Beihang University, Beijing 100191, China*

Abstract Interlocked-ring polymers, also known as polycatenanes, possess an interesting molecular architecture. These polymers are composed of many interlocked rings in a linear chain. The topological constrain between neighboring rings distinguishes the interlocked-ring polymer from its linear counterpart. Here we present extensive molecular dynamic simulations on the interlocked-ring polymers and analyze the static properties of the polymer. By applying external forces to the polymer, we also study the force-extension curves of the polymer, which provides rich information about the mechanical properties of the interlockedring polymers.

Keywords Polycatenanes; Molecular dynamics simulation; Force-extension; Entanglement

Citation: Wu, Z. T.; Zhou, J. J. Mechanical properties of interlocked-ring polymers: A molecular dynamics simulation study. *Chinese J. Polym. Sci.* **2019**, *37*, 1298–1304.

INTRODUCTION

The properties of polymer materials depend on the molecular architecture of polymer chains and various interactions between polymers. Besides the short-range interaction originated from van der Waals interaction which is present for simple fluids, the polymer has one distinct interaction stemmed from the fact that polymer chains cannot pass through each other without breaking the covalent bonds. This topological interaction, or entanglement effect, leads to very different dynamics of long-chain linear polymer in comparison to that of short-chain counterparts.[1,2] One interesting type of polymers is the ring polymer. Since the ring polymers are connected head-to-toe and there are no open ends, the topological interaction is present on the level of individual rings. There are a number of important polymer architectures based on the ring polymers: Olympic gel,[3–5] polyrotaxanes,[6,7] and polycatenanes.[8] Here we focus on the polycatenanes, polymers with a linear chain of many interlocked rings. We will also use the term "interlocked-ring polymers" in the following part of this article.

Naturally, early studies on interlocked-ring polymers are mostly based on computer simulations, because it is much easier to create these complex polymer on computer than in a laboratory. In one of the early studies on the interlocked-ring polymers,[9] Pakula and Jeszka started their paper by stating, "This paper is the first of a series of publications that will present computer-simulated properties of single macromolecules with structures that cannot easily be synthesized by currently known methods." Polymer synthesis has since caught up. Wu *et al*. recently synthesized the interlocked-ring polymers successfully.[10] The connectivity in these interlocked-ring polymer has been maintained by both the traditional covalent bonds that form the individual rings, and the topological bonds that connect the neighboring ring pairs. The interlocked-ring architecture presents an important class of topological interactions. Different from the linear polymer, for which the topological interactions only become important when the chains are longer than the entanglement length, the interlocked-ring polymers possess topological interactions between each pair of neighboring rings. This may lead to new dynamical and mechanical properties of polymeric materials.

There are a few simulation studies on interlocked-ring polymers. Pakula and Jeszka investigated the structure and dynamics of the interlocked-ring polymer using Monte-Carlo simulations based on a lattice-model of the polymer.[9] Rauscher *et al*. used molecular dynamics simulations to study the dynamical behavior of the interlocked-ring polymers.[11] Their Rouse-model analysis showed that the dynamics of interlocked-ring polymer is significantly slowed down on the short length scale. Based on these initial works, here we employ the same polymer model as that in Ref. [11] to study the mechanical properties of the interlocked-ring polymers.

In this work, we study the static and mechanical properties of an isolated interlocked-ring polymer using molecular dynamics simulations. We systematically vary the size of the ring and the total number of interlocked rings. We use Langevin simulations to study the chain conformation in

* Corresponding author: E-mail jjzhou@buaa.edu.cn
Received March 24, 2019; Accepted April 18, 2019; Published online June 4, 2019

equilibrium and under external stretching forces. The remainder of this article is organized as follows: In Section Simulation Details, we present the simulation model for interlocked-ring polymers and describe simulation protocols. We present the simulation results about the static and mechanical properties of isolated chain in Section Results and Discussion. Finally, we conclude in Section Conclusions with a brief summary.

SIMULATION DETAILS

In this section, we introduce the simulation model of interlocked-ring polymers and present the detailed simulation protocols for the measurement of static and mechanical properties.

We employ a bead-spring model proposed by Kremer and Grest[12] to simulate the interlocked-ring polymers. Our system contains n polymer rings and each ring is composed of m beads (or monomers). All beads have the same mass M and diameter σ. Short-range excluded volume interaction between each pair of beads is modeled using the pure repulsive part of the Lennard-Jones interaction (also known as Weeks-Chandler-Anderson potential[13]):

$$U_{\mathrm{LJ}}(r)=\begin{cases}4\varepsilon\left[\left(\frac{\sigma}{r}\right)^{12}-\left(\frac{\sigma}{r}\right)^{6}+\frac{1}{4}\right], & r<\sqrt[6]{2}\sigma\\ 0, & \text{otherwise}\end{cases} \quad (1)$$

where r is the distance between two beads. The interaction parameter ε and the diameter σ characterize the energy and length scales, respectively. Here the shift of the potential ε is chosen so that the potential equals zero at the cutoff $\sqrt[6]{2}\sigma$.

The neighboring beads in each ring are connected by a finitely extensible non-linear elastic (FENE) spring to mimic the covalent bond. This bonded interaction has the form

$$U_{\mathrm{FENE}}(r)=-\frac{1}{2}kR_0^2\ln\left[1-\left(\frac{r}{R_0}\right)\right] \quad (2)$$

where r is the distance between two neighboring beads, k is the spring constant, and R_0 is the maximum distance between two beads. The parameters are chosen as $k=30\varepsilon/\sigma^2$ and $R_0=1.5\sigma$. For these choices, the bond length fluctuates within the equilibrium bond length σ, and events of chain crossing are prohibited.[12] This is important to maintain the interlocked structure during the simulations.

The chain stiffness is simulated using a cosine bond-angle bending potential. This interaction has the form

$$U_{\mathrm{bend}}(\theta)=k_\theta(1+\cos\theta) \quad (3)$$

where θ is the angle between adjacent bonds. The bending constant k_θ is an adjustable parameter which controls the stiffness of the ring polymer. In this work, we have used the value $k_\theta=0.0$, 1.5ε, and 10.0ε to model the flexible, semi-flexible, and rigid chains, respectively. The corresponding persistent lengths are 1.2σ, 2.0σ, and 8.7σ.

In Table 1, we list all simulation variables describing the interlocked-ring polymers in the system and their corresponding value.

We perform Langevin simulations of the interlocked-ring polymers, where the solvent is treated implicitly. The effect of the solvent is incorporated *via* a viscous environment that provides a coupling to a thermal bath in the equations of motions of the beads. The motion of the i^{th} bead is expressed as

$$M\frac{\mathrm{d}^2\mathbf{r}_i}{\mathrm{d}t^2}=-\xi\mathbf{v}_i-\nabla_{\mathbf{r}_i}U+\mathbf{f}_i(t) \quad (4)$$

where M and ξ are the monomer mass and friction coefficient, respectively. The three terms on the right-hand side of Eq. (4) are the frictional force, the conservative force, and the random force, respectively. The coefficient in the frictional force is chosen as $\xi=0.5\tau^{-1}$, where $\tau=\sigma\sqrt{M/\varepsilon}$ is the time unit of the simulation. The term U is the total potential energy, including the excluded volume interaction (1), the FENE bonded interaction (2), and the bending interaction (3). The gradient of the potential gives the conservative force. The force $\mathbf{f}_i(t)$ refers to a random force experienced by the bead, which mimicks the effect of thermal motion due to the surrounding solvents. This random-force term satisfies the fluctuation-dissipation theorem

$$\langle\mathbf{f}_i(t)\cdot\mathbf{f}_j(t')\rangle=\delta_{ij}6k_{\mathrm{B}}T\xi\delta(t-t') \quad (5)$$

Thus, the amplitude of the fluctuation is related to the dissipation term ξ. The temperature of the system is set at $k_{\mathrm{B}}T=1.0\varepsilon$. The time-integration of Eq. (4) is performed using velocity-Verlet scheme.[14–16] A small time step $\Delta t=0.005\tau$ is used for all simulations. All simulations are carried out using the open-source package LAMMPS.[17]

Eq. (4) implies that we have neglected hydrodynamic interactions. Since we are mostly interested in the static equilibrium properties of the systems, the negligence of hydrodynamics seems reasonable.

We consider the cubic simulation boxes with very large box sizes to ensure there is no overlap between chains and their periodic images. We start the simulation with one single interlocked-ring polymer in the center of the box. The initial configuration of the chain is carefully chosen so the topological feature is present. We then perform the Langevin dynamics simulation until the system reaches equilibrium. The equilibration process normally takes 2×10^8 time steps. After equilibration, we take a snapshot and record the position of each bead every 2000 steps in the following 2×10^7 time steps. These trajectories are used to perform a statistical analysis and compute the physical quantities, as presented in the next section.

To study the mechanical properties of the interlocked-ring polymer, we also apply external forces to stretch the polymer. We choose one of the beads in the first ring and one in the last ring randomly, and then apply one pair of the constant forces, same in magnitude but opposite in direction. We start with small forces and run the simulation for 10^6 time steps to reach a steady state. Measurement is performed over the following 10^6 time steps. We then increase the external forces by a small amount and repeat the step again until the maximum forces are reached.

Table 1 Simulation variables and their values

Variable	Symbol	Value
Number of rings	n	10, 20, 50, 100
Number of beads for each ring	m	10, 15, 20, 30
Bending constant	k_θ	0.0, 1.5ε, 10.0ε

https://doi.org/10.1007/s10118-019-2279-z

RESULTS AND DISCUSSION

In this section, we first present the static properties of the interlocked-ring polymer and then attempt to build a coarse-grained model of the interlocked-ring polymer based on the semi-flexible chain model. Finally, we study the mechanical properties of the interlocked-ring polymer and construct the force-extension curves.

Static Properties

The global static properties of the interlocked-ring polymer are characterized by two quantities which relate to the global size of the polymer. One is the end-to-end distance

$$R_e^2 = \langle(\mathbf{r}_1 - \mathbf{r}_N)^2\rangle \quad (6)$$

where $\mathbf{r}_1$ and $\mathbf{r}_N$ are the coordinates for the first bead and the last bead. The total number of beads is denoted by $N = m \times n$. Since for the ring-polymer, there are no chain ends, here we choose the first bead and the last bead randomly in the first ring and the last ring, respectively. The angled brackets indicate the average over time.

The other quantity is the radius of gyration

$$R_g^2 = \frac{1}{N}\left\langle \sum_{i=1}^{N} (\mathbf{r}_i - \mathbf{r}_{com})^2 \right\rangle \quad (7)$$

Here $\mathbf{r}_i$ is the coordinate of the i^{th} bead and $\mathbf{r}_{com}$ is the position of the center-of-mass for the whole molecule.

Fig. 1 shows the end-to-end distance R_e and the radius of gyration R_g for the interlocked-ring polymers with different values of m (number of beads per ring) and n (number of rings). Most of the data points follow the $N^{0.6}$ scaling, which is the scaling for a linear polymer chain in a good solvent. The simulation data shows derivation from the good-solvent scaling at large N number. Possible causes for the deviation include the local chain swelling and excluded volume effects. For linear chains, each monomer has a segmental volume on the order of σ^3. For ring polymers, the chains are connected to form a closed loop, and it is more likely that one bead interacts not only with its neighboring beads but also with other beads that are further away along the chain. Due to this topological constraint of the ring structure, each ring has a higher local segmental density. The increased bead density for ring polymers may cause the interlocked-ring polymer to be more strongly impacted by the excluded volume and thus become stiffer than the linear polymer. This leads to a large scaling factor N^{α} with $\alpha > 0.6$.

For interlocked-ring polymers, we can also analyze the size of individual rings. Fig. 2 shows the radius of gyration for individual rings with different sizes m. All polymers have the same number of rings $n = 100$. Here we also show the results for rings with different bending constants. For flexible rings ($k_\theta = 0$), the ring size increases as a function of $m^{0.6}$, which is the same scaling as the whole molecule. When the bending constant increases, individual ring becomes more rigid. For rigid rings ($k_\theta = 10$), the ring size increases as a function of m^1, which is the scaling for rod-like polymers.

Coarse-grained Model

In this section, we attempt to develop a coarse-grained model for the interlocked-ring polymer. For the interlocked-ring polymer, the connectivity between rings is maintained by the topological constrains that the neighboring rings are interlocked. A convenient choice of the coarse-graining scheme is to map each ring into one single macro-beads. The position of the macro-beads is determined by the center-of-mass location of the corresponding ring. These coarse-grained macro-beads are then connected to form a single linear polymer chain. This procedure is shown schematically in Fig. 3.

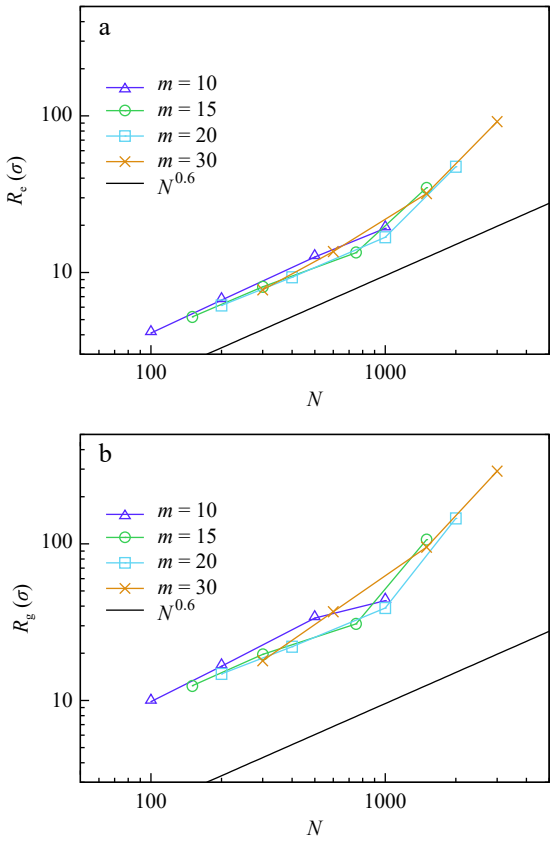

Fig. 1 (a) The end-to-end distance R_e and (b) the radius of gyration R_g for the interlocked-ring polymers with different m (number of beads per ring) and n (number of rings) values. The total number of beads N is given by $N = m \times n$.

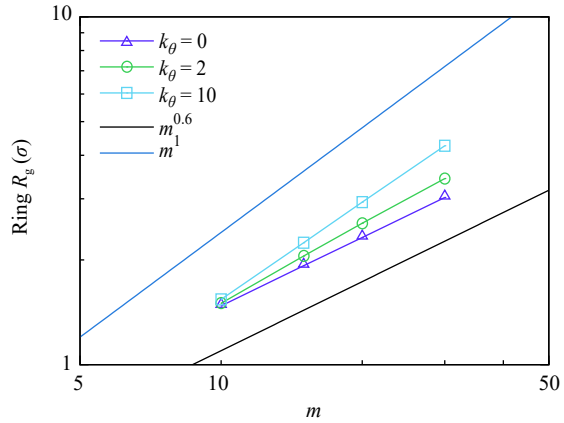

Fig. 2 The radius of gyration R_g for individual rings. Here the simulation data are shown for different m number of beads per ring and k_θ (bending constant).

https://doi.org/10.1007/s10118-019-2279-z

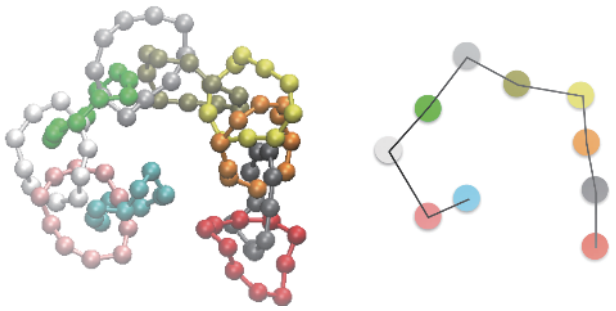

Fig. 3 A coarse-grained model for the interlocked-ring polymer by mapping each ring to a single macro-bead

One possible model for the coarse-grained chain is the worm-like chain model. In the worm-like chain model, one important quantity is the persistent length L_p, which characterizes the stiffness of the chain. For a linear chain consisting of N bonds of the same length L_r, the length of the chain is $L_0 = NL_r$. We use $\mathbf{u}_i$ to denote the unit direction at which the i^{th} bond points, *i.e.*, $\mathbf{u}_i = (\mathbf{R}_{i+1} - \mathbf{R}_i)/|\mathbf{R}_{i+1} - \mathbf{R}_i|$, where $\mathbf{R}_i$ is the position of the i^{th} macro-bead. The angle correction function is given by

$$\langle \mathbf{u}_i \cdot \mathbf{u}_j \rangle = \exp\left(-\frac{|i-j|L_r}{L_p}\right) \tag{8}$$

where the angled brackets denote the average over all starting position and chain configurations. From the angle correlation function we can then calculate the persistent length.

From the trajectory of the interlocked-ring polymer, we apply the coarse-graining scheme to map the polymer as a linear chain of macro-beads. We obtain the bond length L_r by averaging the chain length and configurations at different time. Fig. 4 shows the average bond length L_r of the coarse-grained chain for different ring sizes. The data are collected for interlocked-ring polymers with $n = 100$ rings. Here the bond length L_r denotes the averaged bond length between two neighboring coarse-grained beads, so L_r should be comparable to the radius-of-gyration of the individual ring. Indeed, the bond length curve shown in Fig. 4 demonstrates a similar trend to that of the radius-of-gyration of the ring ($k_\theta = 0$ curve in Fig. 2): both curves show a scaling factor of 0.6 with respect to the ring size m. This agreement provides the validation of our coarse-graining scheme.

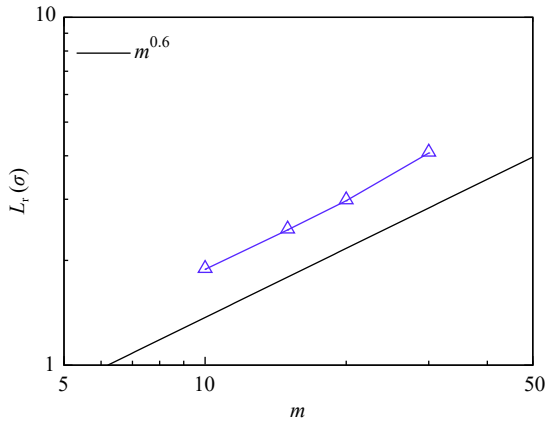

Fig. 4 The average bond length L_r of the coarse-grained chain as a function of the ring size m. Here the data correspond to the interlocked-ring polymers with $n = 100$ rings and $k_\theta = 0$

From the trajectory of the interlocked-ring polymer, we can calculate the angle correlation function by averaging different chain configurations over many times. We plot in Fig. 5 the angle correlation function $\langle \cos\theta \rangle$ as a function of $\Delta n = |i - j|$. Here we focus on two representative results. Fig. 5(a) shows the result for $m = 10$ and $n = 50$, a polymer with relatively small rings. At short distances, the correlation function decays exponentially. At long distances, the correlation function reduces to around zero. A fit to an exponential function gives the persistent length $L_p = 2.43L_r$.

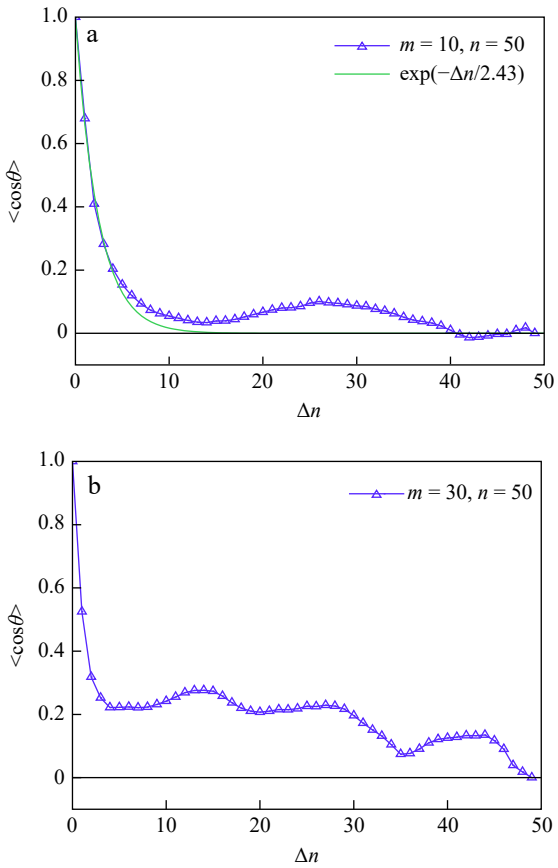

Fig. 5 The angel correlation function <cosθ> for (a) $m = 10$, $n = 50$ and (b) $m = 30$, $n = 50$

For polymer composed of large rings, the angle correlation function shows erratic behavior at long distances. Fig. 5(b) shows the result for $m = 30$ and $n = 50$. The angle correlation function does not decay to zero over a short distance, and $\langle \cos\theta \rangle$ remains at a small positive value over the intermediate distance. This erratic behavior indicates that our coarse-grained model may not be suitable for the polymer with large rings. For the interlocked-ring polymer, the connection between rings derives from topological constraint. There is no fixed point at which two rings are connected, and the connection can move freely along the rings. This is different from the connection by localized covalent bonds in linear polymers. Larger rings occupy larger space, and the nonlocalized connection may cause one ring to influence

https://doi.org/10.1007/s10118-019-2279-z

other rings farther away along the polymer. This might cause the non-zero value of the angle correlation function at the intermediate distance for large rings.

Force-extension Curves

The mechanical properties of the polymer chains are important for their application as advanced materials. Experimentally, the mechanical properties can be probed by applying a pair of constant forces opposite in directions on two chain ends. The resulting force-extension curve can provide detailed information about the mechanical properties. For example, Gaussian chain has a linear force-extension curve

$$F = \frac{3k_BT}{Nb^2}\langle R\rangle \tag{9}$$

where F is the external force, $\langle R\rangle$ is the average end-to-end distance along the force direction, b is the length of Kuhn segments, and N is the number of Kuhn segments. The Gaussian chain behaves similarly to an elastic spring with the spring coefficient of $k = 3k_BT/(Nb^2)$.

Another example is the worm-like chain, which has finite extensibility. The end-to-end distance under stretching is given by the Langevin function:[18]

$$\langle R\rangle = Nb\left[\coth\left(\frac{Fb}{k_BT}\right) - \frac{k_BT}{Fb}\right] \tag{10}$$

For small forces, the term in the square brackets is approximately $Fb/(3k_BT)$, so in this limit, the worm-like chain and the Gaussian chain model have the same force-extension relation. For large forces, this term goes like $1 - k_BT/(Fb)$, and $\langle R\rangle$ approaches its maximum value of Nb.

For interlocked-ring polymers, a typical force-extension curve is shown in Fig. 6(a) for $m = 20$ and $n = 50$. The force-extension curve shows different behaviors at small and large external forces. When the external forces are small, the force-extension curve shows a large slope, indicating a small spring constant. In the small-force regime, the polymer is slightly stretched along the force direction. On the ring level, each ring still has a circular shape and experiences many different configurations. This is demonstrated in the top of Fig. 6(b) for $F = 5\varepsilon/\sigma$. Only part of the chain is shown for clarity. Every ring remains in a relaxed state and its length along the force direction is below the stretching limit.

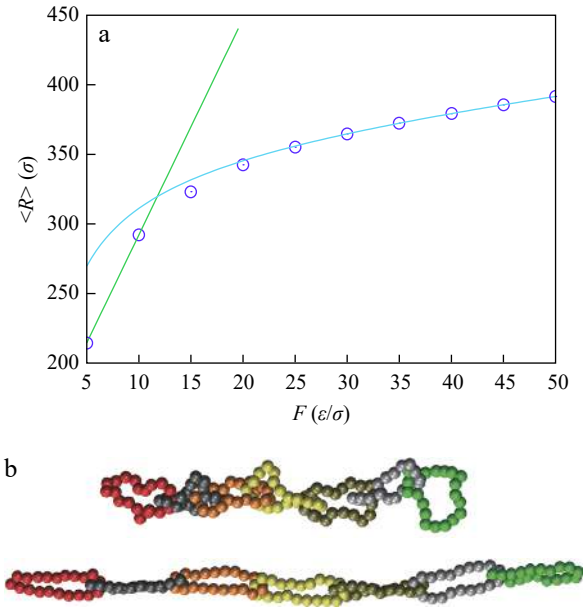

Fig. 6 (a) The force-extension curve for the interlocked-ring polymer with $m = 20$ and $n = 50$. The green and blue curves show the fitting at small-force and large-force regimes, respectively (see the main text for details); (b) Snapshots of chain configuration when the external force is small (top, $F = 5\ \varepsilon/\sigma$) and large (bottom, $F = 50\ \varepsilon/\sigma$). Only a portion of the chain is shown here.

We quantify the initial force-extension curve by fitting a linear function in the regime of small forces. In the small force regime, if the force-extension curve is given by $F = k_{small}\langle R\rangle$, we plot $1/k_{small}$ for different ring sizes and different numbers of rings in Fig. 7. One may apply the coarse-grained model in previous section and consider the whole polymer as linearly connected macro-beads. The average distance between the neighboring macro-beads is given by L_r. When the external force is small, one may expect the linear chain is Gaussian. From Eq. (9), the spring constant would be inversely proportional to the number of rings n and the averaged bond length L_r

$$k_{small} \sim \frac{1}{nL_r} \quad \text{or} \quad \frac{1}{k_{small}} \sim nL_r \tag{11}$$

This is indeed the case shown in Fig. 7. For the same ring size, the $1/k_{small}$ value is linear with respect to the number of rings n. The slope of the curve is larger for large ring size ($m = 30$), which is also consistent with the assumption in Eq. (11).

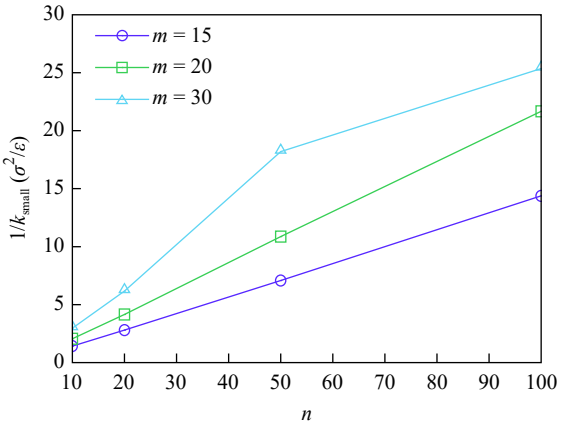

Fig. 7 The spring constants of force-extension curves at the small-force region. The value of $1/k_{small}$ is plotted as a function of ring number n, for different ring sizes m.

When the external force is large, the whole polymer is strongly elongated. Each ring is also strongly stretched along the force direction and shows a rod-like configuration (Fig. 6b, bottom). In this case, every bond in the ring polymer is strongly stretched, contributing to the spring constant. This leads to a small slope in the force-tension curve when the forces are large (Fig. 6a), which corresponds to a large spring constant. At large extension, the force-extension curve can be fitted to the extensive worm-like chain model:[10,19]

$$\langle R\rangle = L_0\left[1-\frac{1}{2}\sqrt{\frac{k_BT}{Fl_p}}+\frac{F}{E}\right] \quad (12)$$

where L_0 is the contour length of the interlocked-ring polymer, l_p is the persistent length, and E is the stretch modulus. The blue curve in Fig. 6(a) shows a fit of Eq. (12) for the large-force portion of the force-extension curve. The fitted curve shows good agreement with the simulation data at large forces, but deviates at small forces.

We perform the fit analysis for the force-extension curves obtained from the simulation. Here we focus on the long chain case $n = 100$ and we also explore the effect of bending rigidity. Fig. 8 shows the parameters L_0, l_p, and E in Eq. (12) by fitting to the simulation results. We plot these parameters as a function of ring size m and for different values of k_θ. The contour length L_0 is proportional to the total number of beads in the polymer, thus for fixed number of rings n, the contour length L_0 shows linear dependency on the ring size m (Fig. 8a). The persistence length is relatively small, on the order of 1 σ (Fig. 8b). Note this persistent length is different from the persistent length obtained in the Section Coarse-grained Model. The former is on the level of individual beads, while the latter is on the level of individual rings. The stretching modulus is related to the extensibility of the polymer chain, which is determined by the bonded interactions in the simulations. Since all the simulations are performed based on the finite extensible non-linear elastic spring with the same parameters, one may expect the stretching moduli are similar for different polymer architectures. The simulation results for the stretching moduli are shown in Fig. 8(c). Indeed the values are close except for small rings with m = 10. In the model of extensive worm-like chain model, the contributions from the bending module and the stretching module are similar, and it is difficult to separate their effect from the force-extension curves. One possible solution is to determine one property from a separate analysis. The coarse-grained model developed in the previous section is our attempt to obtain the bending parameters from the angle correlation functions, but the erratic behavior for large rings (Fig. 5b) made our attempt difficult. Further studies are required to clarify different mechanisms in the large force regime.

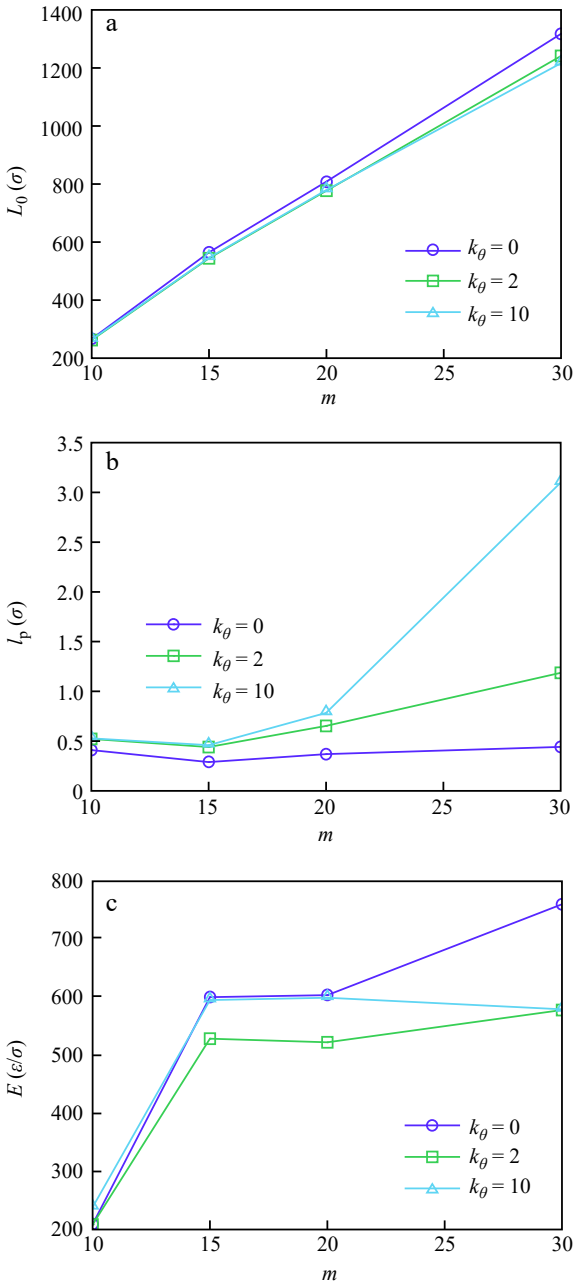

Fig. 8 Mechanical properties of the interlocked-ring polymer at large-force regime. The polymer is modeled as an extensive worm-like chain (12).

CONCLUSIONS

We have performed extensive molecular dynamics simulations of one class of polymer with specific topological interactions: the interlocked-ring polymers. We present the static properties of the polymer and also attempt to build a coarse-grained model for the equilibrium properties. The coarse-grained model seems to work for small ring size but may not be appropriate for large rings due to their expanded size. Our focus is on the mechanical properties of the interlocked-ring polymer. We present the force-extension curves when the polymer is subjected to a pair of external stretching forces.

ACKNOWLEDGMENTS

This work was financially supported by the National students' project for innovation and entrepreneurship training program (No. 201910345046).

REFERENCES

1 de Gennes, P. G. in *Scaling concepts in polymer physics*. Cornell University Press, Ithaca, **1979**.
2 Doi, M.; Edwards, S. F. in *The theory of polymer dynamics*. Clarendon Press, Oxford, **1994**.

3 Lang, M.; Fischer, J.; Sommer, J. U. Effect of topology on the conformations of ring polymers. *Macromolecules* **2012**, *45*, 7642−7648.
4 Lang, M.; Fischer, J.; Werner, M.; Sommer, J. U. Swelling of Olympic gels. *Phys. Rev. Lett.* **2014**, *112*, 238001 .
5 Fischer, J.; Lang, M.; Sommer, J. U. The formation and structure of Olympic gels. *J. Chem. Phys.* **2015**, *143*, 243114.
6 Arunachalam, M.; Gibson, H. W. Recent developments in polypseudorotaxanes and polyrotaxanes. *Prog. Polym. Sci.* **2014**, *39*, 1043−1073.
7 Noda, Y.; Hayashi, Y.; Ito, K. From topological gels to slide-ring materials. *J. Appl. Polym. Sci.* **2014**, *131*, 40509.
8 Niu, Z. B.; Gibson, H. W. Polycatenanes. *Chem. Rev.* **2009**, *109*, 6024−6046.
9 Pakula, T.; Jeszka, K. Simulation of single complex macromolecules. 1. Structure and dynamics of catenanes. *Macromolecules* **1999**, *32*, 6821−6830.
10 Wu, Q.; Rauscher, P. M.; Lang, X. L.; Wojtecki, R. J.; de Pablo, J. J.; Hore, M. J. A.; Rowan, S. J. Poly[*n*]catenanes: Synthesis of molecular interlocked chains. *Science* **2017**, *358*, 1434−1439.
11 Rauscher, P. M.; Rowan, S. J.; de Pablo, J. J. Topological effects in isolated poly[*n*]catenanes: Molecular dynamics simulations and rouse mode analysis. *ACS Macro Lett.* **2018**, *7*, 938−943.
12 Kremer, K.; Grest, G. S. Dynamics of entangled linear polymer melts: A molecular-dynamics simulation. *J. Chem. Phys.* **1990**, *92*, 5057.
13 Weeks, J. D.; Chandler, D.; Andersen, H. C. Role of repulsive forces in determining the equilibrium structure of simple liquids. *J. Chem. Phys.* **1971**, *54*, 5237.
14 Swope, W. C.; Andersen, H. C.; Berens, P. H.; Wilson, K. R. A computer simulation method for the calculation of equilibrium constants for the formation of physical clusters of molecules: Application to small water clusters. *J. Chem. Phys.* **1982**, *76*, 637.
15 Allen, M. P.; Tildesley, D. J. in *Computer simulation of liquids*. 2nd ed., Clarendon Press, Oxford, **2017**.
16 Frenkel, D.; Smit, B. in *Understanding molecular simulation*. 2nd ed., Academic Press, **2002**.
17 Plimpton, S. Fast parallel algorithms for short-range molecular dynamics. *J. Comput. Phys.* **1995**, *117*, 1−19.
18 Rubinstein, M.; Colby, R. H. in *Polymer physics*. Oxford University Press, Oxford, **2003**.
19 Odijk, T. Stiff chains and filaments under tension. *Macromolecules* **1995**, *28*, 7016−7018.

https://doi.org/10.1007/s10118-019-2279-z